



Article

Ocean Wind and Current Retrievals Based on Satellite SAR Measurements in Conjunction with Buoy and HF Radar Data

He Fang ¹, Tao Xie ^{1,*} , William Perrie ², Li Zhao ¹, Jingsong Yang ³ and Yijun He ¹ 

¹ School of Marine Sciences, Nanjing University of Information Science and Technology, Nanjing 210044, Jiangsu, China; fanghe_doc@163.com (H.F.); nuist-zhaoli@foxmail.com (L.Z.); yjhe@nuist.edu.cn (Y.H.)

² Fisheries & Oceans Canada, Bedford Institute of Oceanography, Dartmouth, NS B2Y 4A2, Canada; william.perrie@dfo-mpo.gc.ca

³ State Key Laboratory of Satellite Ocean Environment Dynamics, Second Institute of Oceanography, State Oceanic Administration, Hangzhou 310012, Zhejiang, China; jsyang@sio.org.cn

* Correspondence: xtplqk@126.com; Tel.: +86-255-869-5697

Received: 22 September 2017; Accepted: 13 December 2017; Published: 15 December 2017

Abstract: A total of 168 fully polarimetric synthetic-aperture radar (SAR) images are selected together with the buoy measurements of ocean surface wind fields and high-frequency radar measurements of ocean surface currents. Our objective is to investigate the effect of the ocean currents on the retrieved SAR ocean surface wind fields. The results show that, compared to SAR wind fields that are retrieved without taking into account the ocean currents, the accuracy of the winds obtained when ocean currents are taken into account is increased by 0.2–0.3 m/s; the accuracy of the wind direction is improved by 3–4°. Based on these results, a semi-empirical formula for the errors in the winds and the ocean currents is derived. Verification is achieved by analysis of 52 SAR images, buoy measurements of the corresponding ocean surface winds, and high-frequency radar measurements of ocean currents. Results of the comparisons between data obtained by the semi-empirical formula and data measured by the high-frequency radar show that the root-mean-square error in the ocean current speed is 12.32 cm/s and the error in the current direction is 6.32°.

Keywords: ocean currents; polarization; ocean surface wind; synthetic-aperture radar

1. Introduction

Ocean surface currents are a defining feature of the interactions between the ocean and the atmosphere. Almost all ocean processes can be related to the ocean currents, making them an important physical parameter for marine meteorology and physical oceanography [1]. Observations of the ocean currents can enhance our understanding of the physical mechanisms of atmospheric–oceanic interactions and our ability to improve numerical weather predictions (NWP) model forecasts. Therefore, near-real time sea surface current information is needed for ocean operations [2]. Thus far, methods for measuring ocean surface currents can be classified into two categories: direct measurements and remotely sensing measurements. Direct measurements are mainly achieved by buoys and electromagnetic current meters, which have the disadvantage that they can only report data at a relatively few sampling locations, often with limited coverage in time, difficulty and expense in deploying instruments, and vulnerability to severe environmental conditions. With improved remote sensing techniques in recent years, the monitoring of surface currents has greatly improved, making it possible to even perform real-time observations over extended areas of the sea surface [3]. Among these techniques, SAR has become a new technical means to observe ocean surface features because of its high resolution and capacity to operate in almost all weather conditions, day or night [4,5].

SAR can observe a variety of ocean surface phenomena by measuring the backscatter resulting from the radar’s electromagnetic waves from the ocean surface. Among these, are ocean surface currents which can be derived from fully polarimetric SAR images [6–8]. Moreover, some studies suggest that ocean surface currents also have significant effects on the electromagnetic backscattering signals per se, and therefore on the retrievals of associated ocean surface parameters [9,10]. Estimates of the wind stress, as determined from wind speed measurements retrieved from conventional radar scatterometers mounted on satellites, are usually derived neglecting ocean currents. Moreover, the scatterometer measures relative motion, not wind alone. Therefore, the scatterometer-derived wind stress is a more accurate representation of the boundary conditions needed for both atmospheric and oceanic models than stress fields derived neglecting ocean currents [11]. In terms of global averages, ocean winds are about 6 m/s and the downwind (or upwind) currents in the same ocean area are on the order of 0.3 m/s. It is known that modulations of wind stress by downwind and upwind ocean currents can result in differences that are typically 10%, and can reach 20% in strong currents [12]. There are two processes by which ocean currents can affect wind stress. One process is that the ocean surface current per se changes the surface relative wind speed of the wind, which changes the effective wind stress. A second process is that the sea surface temperature (SST) gradients change the stability of air-sea boundary layer and the associated wind field near the ocean surface. When the wind passes over an SST frontal area, the associated acceleration and deceleration that is experienced causes convergence and divergence of the wind stress, which are linearly correlated with along-wind and cross-wind SST gradients, respectively [13,14].

The accuracy of wind data retrieved from SAR images is closely related to the normalized radar cross section (NRCS). Previously, we have shown that ocean surface currents have a significant influence on the backscatter of electromagnetic (EM) signals and may be relevant to SAR measurements. According to this approach [15], the one-dimensional linear wave-current fractal ocean surface is

$$y' = f(x', t) = \sum_{n=0}^{N-1} \sigma C b^{(s-2)n} \left(1 - \frac{k_0 b^n}{\omega_n} C_0 \right) \times \sin(k_0 b^n x' - \omega_n t + \varphi_n) \tag{1}$$

where $\omega_n = \sqrt{gk_n}$ is the dispersion relationship; $k_0 = 2\pi/\lambda_0$ is the dominant ocean wave number, λ_0 is the dominant wavelength; b ($b > 1$) is the scale factor for amplitude and frequency; σ is the standard deviation of $f(x, t)$ which is related to the significant wave height h_s by $\sigma = h_s/4$; $C = \sqrt{\frac{2[1-b^{2(s-2)}]}{1-b^{2N(s-2)}}$, and s ($1 < s < 2$) is the roughness coefficient of the fractal sea surface. Here, $k_n = k_0 b^n$, ω_n , φ_n are wave number, the radian frequency and the phase of the n -th wave components, respectively. The dispersion relation for the coupled wave–current dynamics in deep water can be written as $(\omega - kC_0)^2 = kg$, where $g = 9.8$ m/s is the acceleration due to gravity. After some mathematical manipulation, the EM backscatter coefficient for the coupled wave-current fractal sea surface is as [15]

$$\gamma(t) = \frac{1}{L \cos^2 \theta} \sum_{p=-\infty}^{\infty} \prod_{n=0}^{N-1} J_{p_n} \left[-2\sigma k_{em} C b^{(s-2)n} \times \left(1 - \frac{k_0 b^n}{\omega_n} C_0 \right) \cos \theta \right] \times \text{sinc} \left[\left(k_{em} \sin \theta + \frac{1}{2} \sum_{n=0}^{N-1} p_n k_0 b^n \right) L \right] e^{j p^T \zeta(t)} \tag{2}$$

where L denotes the fractal sea surface over which the surface integration is carried out where $x \in [-L/2, L/2]$, Bessel functions are $J_p(u)$, and p ($p_0, p_1, p_2, \dots, p_{N-1}$)^T, $p_n = -\infty, \dots, -2, -1, 0, 1, 2, \dots + \infty$; $\zeta(t) = [\zeta_0(t), \zeta_1(t), \zeta_2(t) \dots \zeta_{N-1}(t)]$ ^T. For remote sensing with RADARSAT-2 SAR, this latter equation suggests that we can calculate the NRCS of the fractal sea surface with the following expression:

$$\sigma_0 = 2 \log_{10} \gamma \tag{3}$$

where the frequencies of the transmitter and receiver are both $f = 5.4$ GHz; the electromagnetic wavenumber is $k = 2\pi f/v$, where $v = 3 \times 10^8$ m/s. Letting $N = 25$, $s = 1.3$, $b = 2e/3$, and dominant

wavelength $\lambda_0 = 200$ m, then the dominant wavenumber is given by $k_0 = 2\pi/\lambda_0$. Assuming sea state conditions where significant wave heights of 2 m, σ is taken as 0.5, and the illumination area is $L = 10\lambda_0$.

To find the effect of ocean currents on the EM backscatter of the fractal sea surface, the above parameters are applied to our EM backscatter model for an assumed 1D drifting fractal sea surface. As an example, the ocean current velocities are assumed to range from -1.5 m/s to 1.5 m/s in steps of 0.5 m/s in our simulations. The NRCSs of these wave–current effects in the coupled ocean surface model, with incidence angles ranging from 0° to 70° , have been computed in our previous work [16]. Obviously, the NRCS is different when the incidence angle has a fixed value.

Based in the approach given above, we analyzed full polarimetric SAR images, the buoy measurements of surface wind vectors and high-frequency radar measurements of ocean surface currents to investigate the effect of the currents on the retrieved SAR winds. We will show that sea surface currents are a factor that causes error in the accuracy of the SAR retrieval wind field. Thus, a semi-empirical formula for associated modifications, or differentials, in the wind fields and surface currents are derived for the retrieval of the sea surface current field.

2. Data and Methods

2.1. Satellite, Buoy, and High-Frequency Radar Data

Three types of data are used in this paper to analyze the effects of ocean currents on the winds retrieved from SAR images. They are radar backscatter from fully polarimetric SAR observations, winds from the National Data Buoy Center (NDBC) buoys and ocean currents from the Scripps Institution of Oceanography (SIO) High Frequency Radar National Network (HFRnet). Ocean wind speeds and directions are retrieved from RADARSAT-2 fine quad polarization SAR data. Ocean surface currents are measured by HF radar, including speeds and directions, which are overlain on the retrieved wind fields. Collocated co-temporal NDBC buoy data are used to validate the effectiveness of our experiment.

In this approach, we used RADARSAT-2 SAR measurements as the source of the remotely sensed wind data. RADARSAT-2 SAR data have multiple polarization modes, including a fully polarimetric mode in which HH, VV, HV, and VH polarized data are acquired [17]. For the purpose of retrieval of ocean wind speed and direction, we selected the fine quad polarization mode. Because of the complex scattering coefficients (S_{VV} and S_{VH}) used in our retrieval method, the single-look complex (SLC) product type are used. $\text{Real}(\rho_{VVVH})$ and $\text{Imag}(\rho_{VVVH})$ are complex magnitudes which correspond to the real and imaginary parts of the scattering coefficients in the SLC products, respectively. To analyze the effects of ocean currents on retrieved wind vectors, we collected RADARSAT-2 images and collocated buoy and HF radar data from geographic locations located on the East and West Coasts of the USA, Gulf of Alaska, and the Gulf of Mexico. The NDBC (<http://www.ndbc.noaa.gov/>) buoy data are co-temporal and collocated with the SAR images. Each individual SAR image covers one NDBC buoy. Buoy measurements also include meteorological parameters (SST, wind speed, wind directions, and related variables) and wave information (such as wave period, wave direction, wave height). The wind speed measurements are adjusted to a height of 10 m. In addition, buoy measurements and the RADARSAT-2 observations are required to occur within a time difference of 30 min.

Ocean currents play significant roles in the transportation of mass, nutrients, momentum, and heat [18]. Shore-based high-frequency (HF) radars with operating frequencies of 3–50 MHz are routinely used for remote sensing of coastal ocean surface currents [19]. The Integrated Ocean Observing System (IOOS) high frequency radar network (HFRnet, <http://hfrnet.ucsd.edu/thredds/catalog.html>) provides continuous, wide-area ocean current observations in real-time over large coastal areas, with ranges up to 200 km off the coastline. In IOOS, there are primarily two types of HF radars, the Coastal Ocean Dynamics Application Radar (CODAR) and the Wellen Radar (WERA). CODAR long-range SeaSonde radars use a compact directional antenna system consisting of three antenna elements in a single housing for receiving backscatter signals and a separate omnidirectional antenna

for transmitting frequency-modulated interrupted continuous radar pulses (FMICW). A WERA system is composed of two separate antenna arrays, one for receiving and the other for transmitting frequency-modulated, continuous wave chirps [20,21]. The HFRnet systems measure the speed and direction of ocean surface currents in near real time. Starting with about 30 radars in 2005, the network has grown to over 130 radars with 33 participating organizations and approximately 10 million radial files [22]. Current speeds and directions provided by these observations are averaged over 1 h periods. Accuracies of the radar-derived velocities have been shown to be typically in the range 5–10 cm/s, as reported in numerous studies. This program covers almost all of the coastal oceans of the United States and including the Great Lakes, East and West Coasts, Hawaii, and the gulfs of Alaska, Maine, and Mexico [23].

2.2. Retrieval Method of Winds from Radarsat-2 SAR Images

The ocean backscatter in cross and co-polarizations are quite different. Cross-polarization is essentially independent of wind direction and local incidence angle but has a linear relationship with respect to wind speed [24]. A C-band cross-polarized ocean backscatter model (C-2PO) relating NRCS in VH polarization σ_{VH}^0 to equivalent neutral wind speed U_{10} at 10-m height reference height, has been developed using RADARSAT-2 fine quad-polarization mode SAR data and collocated buoy observations [25,26]. RADARSAT-2 fine quad-polarization mode SLC SAR data are characterized by a nominal spatial resolution of 8.0×5.4 m in azimuth and range. For each quad-polarization image with a specific beam mode, the pixel spacing in range and azimuth directions is about 5 m. SAR backscatter signals consist of the backscattered radar signal plus the receiver noise. By subtracting the noise component, and related analysis, the C-2PO model is

$$\sigma_{VH}^0 = 0.580 \times U_{10} - 35.652 \quad (4)$$

where U_{10} is the wind speed at 10 m reference height and σ_{VH}^0 is the NRCS of the VH polarization signals. The units of U_{10} and σ_{VH}^0 are in meters per second and decibels, respectively.

Equation (4) can be used to estimate the wind speed. Using the retrieved wind speed and in situ radar incidence angles, we can retrieve wind directions with ambiguities; in this approach, the wind speeds and incidence angles are used as input to the geophysical model function (GMF) called CMOD5.N, as described by [27]. The formulation for CMOD5.N is

$$\sigma_{VV}^0(\theta, U_{10}, \phi) = A_0(\theta, U_{10})[1 + A_1(\theta, U_{10}) \cos \phi + A_2(\theta, U_{10}) \cos 2\phi]^{1.6} \quad (5)$$

where θ , U_{10} , and ϕ are the radar incidence angles, the wind speed, and the relative direction, respectively. Here, A_0 , A_1 , and A_2 are coefficients which are dependent on the radar incidence angle and the wind speed.

Real and imaginary parts of the polarimetric correlation coefficient (PCC) have odd symmetry with respect to wind direction. For satellite SAR, this odd symmetry of the observed polarimetric active backscatter agrees with theoretical considerations from rigorous derivations using the Maxwell's equations, two-scale models, and other earlier airborne polarimetric scatterometer observations [28–30]. To solve the problem of the wind direction ambiguity, the odd-symmetry property is applied to remove the wind direction ambiguities in the C-2PO model. Thus, the correlation between VV and VH polarization channels is defined by the PCC as

$$\rho_{VVVH} = \frac{\langle S_{VV} \cdot S_{VH}^* \rangle}{\sqrt{\langle |S_{VV}|^2 \rangle \langle |S_{VH}|^2 \rangle}} \quad (6)$$

where S_{VV} is the scattering coefficient of vertical transmitting and vertical receiving polarized backscatter, S_{VH}^* is the complex conjugate of S_{VH} which is the scattering coefficient of vertical transmitting and horizontal receiving polarized backscatter. It should be pointed out that PCC

(ρ_{VVVH}) is a complex number that indicates the degree of correlation and the relative phase angle of VV and VH polarized backscatter signals.

Zhang et al. [31] utilized PCC's odd characteristic to derive the criteria to facilitate the selection of the relative wind direction among the possible values: \emptyset , $180 - \emptyset$, $180 + \emptyset$ and $360 - \emptyset$. The criteria are

$$\text{Real}(\rho_{VVVH}) < 0, \text{Imag}(\rho_{VVVH}) > 0, -180^\circ < \phi < -90^\circ;$$

$$\text{Real}(\rho_{VVVH}) > 0, \text{Imag}(\rho_{VVVH}) > 0, 90^\circ < \phi < -0^\circ;$$

$$\text{Real}(\rho_{VVVH}) < 0, \text{Imag}(\rho_{VVVH}) > 0, 0^\circ < \phi < 90^\circ;$$

$$\text{Real}(\rho_{VVVH}) < 0, \text{Imag}(\rho_{VVVH}) > 0, 90^\circ < \phi < 180^\circ.$$

where Real and Imag denote the real and imaginary parts of ρ_{VVVH} , respectively.

To summarize what has been mentioned above, the flowchart for retrieval of the wind field is given in Figure 1.

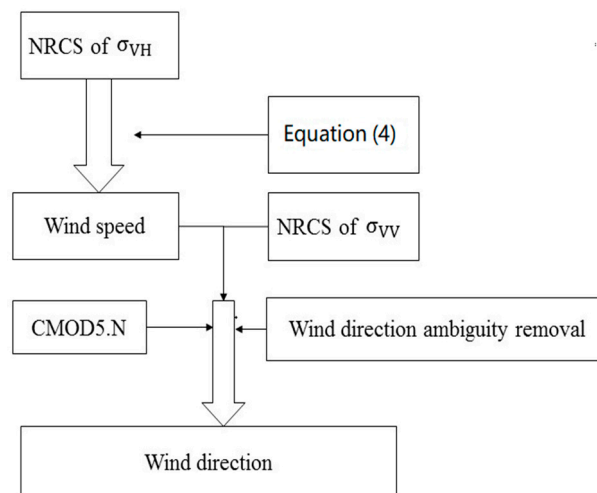


Figure 1. Flowchart for the wind speed and direction retrieval algorithm.

2.3. Validation Method for the Effect of Ocean Currents on the Winds Retrieved from SAR

The following scheme is an outline of the validation using our method:

- (1) RADARSAT-2 fine quad-polarization mode SLC SAR data are characterized by a nominal spatial resolution of 8.0×5.4 m in azimuth and range and the pixel spacing in range and azimuth directions is about 5 m. We make a 20×20 pixel boxcar average on the NRCS, in each polarization, so that the resampled pixel spacing is 100 m.
- (2) Extract geophysical parameters and SAR system information from quad-polarization RADARSAT-2 SAR images, such as longitude, latitude, incident angles, and other information for each pixel, track angle, radar look direction.
- (3) Use MATLAB to obtain the NRCS for VV, VH polarization images, and complex backscattering coefficients S_{VV} , S_{VH} for each pixel, for each SAR image.
- (4) Firstly, we use the NRCS for VH polarization data to calculate wind speed at 10-m reference height (U_{10}) from Equation (4). Secondly, we use the NRCS for VV data to calculate wind direction with ambiguities from Equation (5). Finally, using the directional ambiguity removal criteria previously mentioned, the final wind directions are obtained without ambiguities.
- (5) Collect ocean currents from HF radar and observed wind fields from NDBC buoys in the same location and time as the SAR images.

- (6) Analyze two groups of experiments. In the first group, directly retrieved winds (including wind speed and directions) from SAR are compared to the winds obtained from the corresponding buoy data and the errors are calculated. In the second group, the ocean current information (including the current speeds and directions), are overlaid on wind fields retrieved from SAR images, again compared with the corresponding winds observed by buoys, and the errors are calculated. By comparing the errors calculated in both groups, the impact of ocean currents on the winds retrieved from SAR images at the sea surface can be estimated.

It is important to note that the three data sets used for the matching analysis, namely RADARSAT-2 SAR image data, wind vectors measured by NDBC buoys, and ocean current data observed by HF radar must be simultaneous and collocated. Generally, for spatial collocation, two points on the ocean surface must be less than 2 km apart. If the time interval for obtaining sea surface information is less than 30 min, two events in time can be deemed as occurring at the same time.

3. Results and Discussion

3.1. Effect of Ocean Currents on the Retrieval of Sea Surface Wind from SAR

We selected 168 RADARSAT-2 fully polarimetric SAR images for this part of the study. Each SAR image is collocated and cotemporal with buoy wind vector measurements and HF radar measurements of ocean surface current data. The RMS difference between of the wind speeds retrieved from the selected 168 SAR images and the wind speeds from the buoy data is 1.62 m/s (Figure 2a). The RMS difference between the wind directions derived from SAR data and those derived from buoy data is 15.87° (Figure 2c). When the ocean currents vectors observed by the HF radar are overlaid on SAR retrieved wind fields, the RMS difference between the SAR-derived wind speeds and the buoy data is 1.28 m/s (Figure 2b) and for the wind direction, 12.26° (Figure 2d). In other words, if the ocean currents are considered in the retrieval of wind fields from SAR data, then the retrieved accuracy of the wind speed is improved by about 0.3 m/s and for the wind direction, by about 3°.

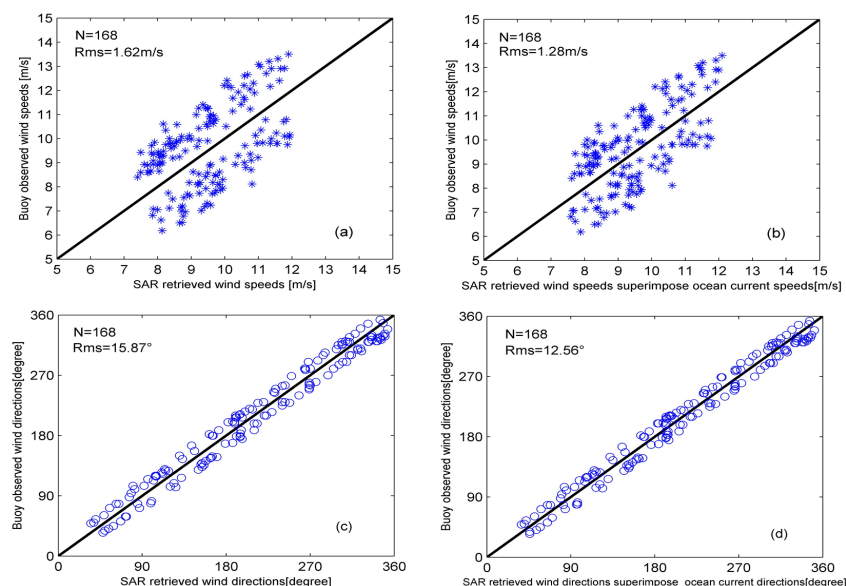


Figure 2. (a) SAR-retrieved wind speeds from C-2PO model compared to wind speeds observed by buoy measurements; (b) SAR-retrieved wind speeds with superimposed ocean current speeds compared to winds speeds observed by buoys; (c) SAR-retrieved wind directions derived from applying the C-2PO model compared to wind directions observed by buoys; (d) SAR-retrieved wind directions with superimposed ocean current directions compared to wind directions observed by buoys.

3.2. Ocean Current Vector Retrieval from Empirical Formulae

If ocean surface currents are taken into account when surface winds are retrieved from fully polarimetric SAR images, the accuracy of the wind speed is improved by 0.3 m/s and the accuracy of the wind direction, by 3°. Therefore, the error in vector winds retrieved from SAR images relative to the actual wind vectors, namely the difference wind fields (DWF), is partially caused by the ocean surface currents. From our analysis of 168 fully polarimetric SAR images and the data from corresponding observed buoy wind vectors and HF radar measurements of ocean surface currents, we have estimated the DWF. Thus, we can linearly fit the DWF vector with the vector of the sea surface currents measured by the HF radar to derive an empirical formula. Thereafter, 52 SAR images are reselected to make the sea surface wind field inversion by using the above mentioned model. The empirical formula is used to obtain the sea surface current vectors.

3.2.1. Empirical Formulae of Ocean Currents and DWF Vector

The vector wind fields, denoted \vec{U}_{SAR} , retrieved from SAR are decomposed into an east–west component U_{SAR} and a north–south component V_{SAR} , using a Cartesian coordinate system (positive X-axis points east and positive Y-axis points north), and the wind direction is represented by \varnothing_{SAR} . Similarly, vector winds measured by the buoys, denoted \vec{U}_{Bouy} , are decomposed as U_{Bouy} (east–west) and V_{Bouy} (north–south), with wind direction represented as \varnothing_{Bouy} . The currents, denoted as \vec{U}_{Sea} , are decomposed into U_{Sea} and V_{Sea} , and the current directions are represented as \varnothing_{Sea} .

As can be inferred from the definition, the differential wind field is the partial error between the vector winds retrieved from SAR data and the vector winds measured by buoys, i.e., $\vec{U}_{Dif} = \vec{U}_{Bouy} - \vec{U}_{SAR}$. Thus, the east–west component can be represented as $U_{Dif} = U_{Bouy} - U_{SAR}$, and the north–south component can be represented as $V_{Dif} = V_{Bouy} - V_{SAR}$. For the 168 fully polarimetric SAR images, we retrieve the wind field information U_{SAR} and V_{SAR} , the corresponding buoy wind vectors U_{Bouy} and V_{Bouy} , and the HF radar measurements of ocean surface currents, U_{Sea} and V_{Sea} . Thus, the relation between the east–west DWF velocities and the radar-measured current velocities can be obtained, as shown in Equation (7); the relation between the north–south DWF velocities and the radar measured current velocities is shown in Equation (8). Figure 3 gives the corresponding scatter diagrams.

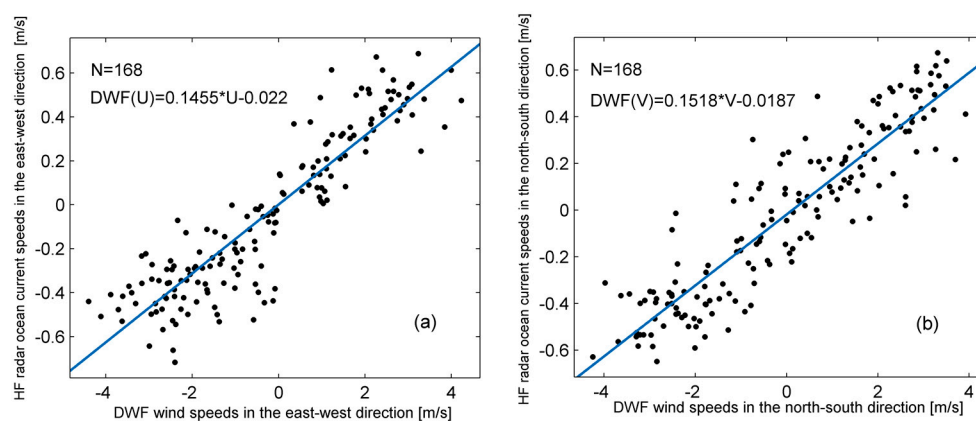


Figure 3. Scatter diagrams between the DWF velocities and HF radar ocean current velocities, in which, U and V represent the east–west and the north–south DWF velocities, respectively; DWF(U) and DWF(V) represent the east–west and the north–south ocean surface current velocities measured by the HF radar.

$$DWF(U) = 0.1455 \times U - 0.022 \quad (7)$$

$$\text{DWF}(V) = 0.1518 \times V - 0.019 \quad (8)$$

3.2.2. Cases of Retrieved Ocean Currents

The first example is a quad-polarization SAR image acquired on 9 January 2012, at 03:52:26 Coordinate Universal Time (UTC). This SAR image collocates with a NDBC buoy (#46035, $57^{\circ}1'33''$ N $177^{\circ}44'16''$ W) in the Bering Sea. The buoy-measured 10-m equivalent neutral wind speed and wind direction are $|\vec{U}_{\text{Bouy}}| = 11.5$ m/s and $\varnothing_{\text{Bouy}} = 266^{\circ}$ at 03:50 UTC.

Following our methodology as described above, we first use the quad-polarization SAR image to calculate the complex backscatter coefficients, S_{VV} and S_{VH} , for each pixel. Therefore, the NRCS values are $\sigma_{VV} = |S_{VV}|^2$ and $\sigma_{VH} = |S_{VH}|^2$. The NRCS images in VV polarization and VH polarization, corresponding to the SAR image are shown in Figure 4. The parameters extracted for this SAR image for ocean surface wind fields are as follows: the wind speed $|\vec{U}_{\text{SAR}}| = 9.85$ m/s and the wind direction $\varnothing_{\text{SAR}} = 252^{\circ}$. These are shown in Figure 5a.

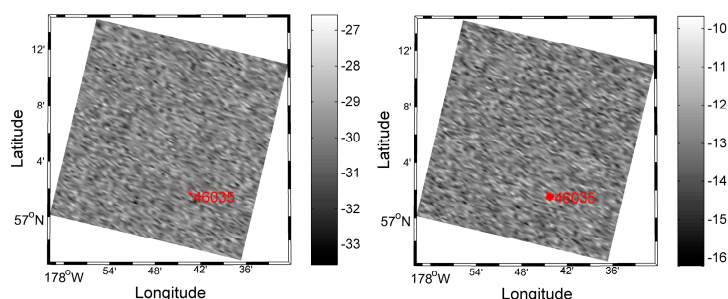


Figure 4. RADARSAT-2 SAR image of the Bering Sea at 03:52:26 on 9 January 2012 showing VH polarization (left) and VV polarization (right). The location of NDBC buoy 46,035 is indicated.

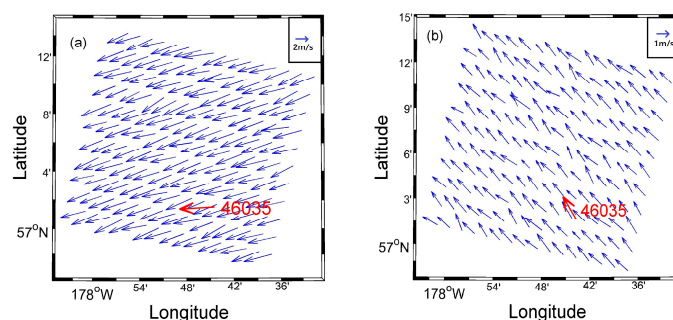


Figure 5. (a) SAR-retrieved wind speed using the C-2PO model and retrieved wind directions without ambiguities derived from PCC between the VV and VH channels; (b) DWF wind speeds and wind directions.

The vector winds retrieved from the SAR images, \vec{U}_{SAR} , are decomposed in the Cartesian coordinate system described above. Thus, the east–west component is $U_{\text{SAR}} = -9.37$ m/s and the north–south component is $V_{\text{SAR}} = -3.04$ m/s. For vector winds taken from the buoy measurements, \vec{U}_{Bouy} , the east–west component is $U_{\text{Bouy}} = -11.47$ m/s, and the north–south component is $V_{\text{Bouy}} = -0.82$ m/s. In this paper, the DWF vectors are defined as the differences between the buoy wind field vectors and the wind field vectors retrieved from the SAR images. Therefore, the east–west DWF is $U_{\text{DWF}} = U_{\text{Bouy}} - U_{\text{SAR}} = -2.11$ m/s, and the north–south differential wind velocity is $V_{\text{DWF}} = V_{\text{Bouy}} - V_{\text{SAR}} = 2.2$ m/s. Therefore, the resulting speed of the DWF synthesized vector is given by $|\vec{U}_{\text{DWF}}| = 3.04$ m/s and for direction, $\varnothing_{\text{DWF}} = 316^{\circ}$ (Figure 5b).

According to the empirical Equations (7) and (8), the east–west and the north–south components of the ocean surface current vector are $U_{re} = -0.28$ m/s and $V_{re} = 0.31$ m/s, respectively. Thus the speed of the synthesized ocean current vector is $|\vec{U}_{re}| = \sqrt{U_{re}^2 + V_{re}^2} = 0.42$ m/s, with the direction, $\varnothing_{re} = 306.2^\circ$. These results are given in Figure 6. The current speed measured by the HF radar at the same time and location is $|\vec{U}_{HF}| = 0.478$ m/s, and the current direction is $\varnothing_{HF} = 311.8^\circ$. The error in the retrieved current speed is 0.072 m/s and the error in the current direction is 5.6° . These results are shown in Table 1.

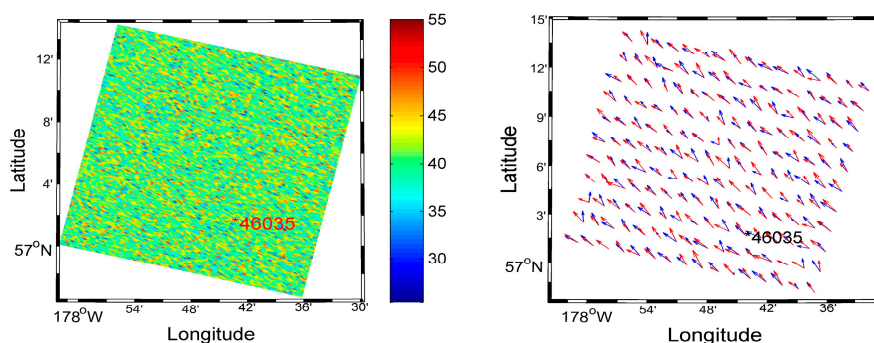


Figure 6. Distribution map for retrieved ocean currents (**left:** units are centimeters per second) and directions (**right:** units are degrees, blue vectors are retrieved-ocean directions and red vectors are measured by HF radar, respectively). The ocean current speed is 42 cm/s and corresponding current direction is 317.6° at buoy #46035.

Table 1. Winds retrieved from fully polarimetric SAR images and NDBC buoy #46035, ocean surface currents measured by HF radar and retrieved ocean currents. Parameters of four kinds of data are simultaneous and collocated. Data are received on 9 January 2012.

	SAR Image	Buoy Data	HF Radar	Retrieval Currents
Time	03:52	03:50	04:00	03:50
Site	57.036° N 177.64° W	57.026° N 177.74° W	57.020° N 177.68° W	57.026° N 177.74° W
Wind/current speed	Wind speed 9.85 m/s	Wind speed 11.5 m/s	Current speed 0.478 m/s	Current speed 0.406 m/s
Wind/current direction	Wind direction 252°	Wind direction 266°	Current direction 323.4°	Current direction 317.6°

The second SAR image was acquired on 19 January 2013, at 02:12 UTC. This SAR image collocates with a NDBC buoy #LKWF1 ($26^\circ 36' 46''$ N, $80^\circ 2' 2''$ W) off the U.S. Southeast Coast, off Florida. The buoy-measured 10 m equivalent neutral wind direction and speed are $\varnothing_{\text{Buoy}} = 57^\circ$ and $|\vec{U}_{\text{Buoy}}| = 8.9$ m/s at 02:10 UTC.

Using the same verification procedures as applied in Case 1, the VH and VV polarized radar backscatter coefficients were determined, as shown in Figure 7. The resulting incidence angle and wind speed at each pixel are substituted into CMOD5.N to calculate the wind direction, with ambiguities. Using the directional ambiguity removal criteria previously mentioned, the final wind direction, without ambiguities, is then calculated. The wind speed retrieved from the SAR image is $|\vec{U}_{\text{SAR}}| = 10.52$ m/s and wind direction, $\varnothing_{\text{SAR}} = 41^\circ$ as shown in Figure 7c. The speed of the DWF synthesized vector $|\vec{U}_{\text{DWF}}|$ is 3.14 m/s and the direction \varnothing_{DWF} is 169.6° as shown in Figure 7d.

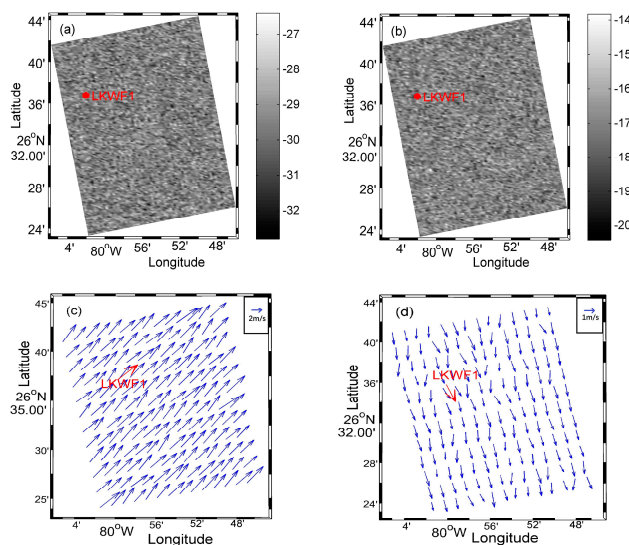


Figure 7. RADARSAT-2 SAR image in the North Atlantic, off Florida, at 02:12:56 on 19 January 2013, collocated with NDBC buoy LKWF1 showing: (a) VH polarization; (b) VV polarization; (c) SAR-derived wind fields; and (d) DWF wind fields.

According to the empirical formula from Section 3.2.1, the east–west and the north–south components of the sea current vector are $U_{re} = -0.059$ m/s and $V_{re} = 0.037$ m/s, respectively. Thus, the speed of the synthesized ocean current vector is $|\vec{U}_{re}| = \sqrt{U_{re}^2 + V_{re}^2} = 0.38$ m/s and the direction is $\varnothing_{re} = 171^\circ$, as indicated in Figure 8. The current speed measured by the HF radar at the same time and location is $|\vec{U}_{HF}| = 0.465$ m/s, and the current direction is $\varnothing_{HF} = 177.2^\circ$. The error in retrieval of the speed is 0.085 m/s and the error in the current direction is 6.2° . All the data are shown in Table 2.

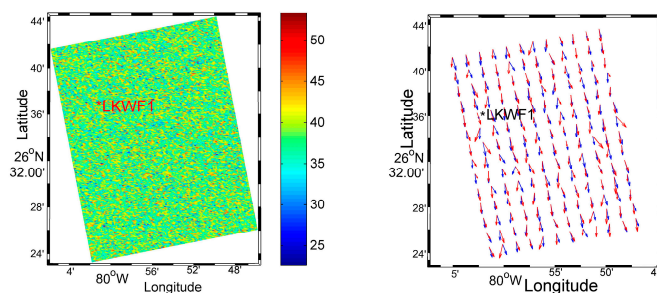


Figure 8. Retrieved-ocean current (left) and directions (right, blue vectors are retrieved-ocean directions and red vectors are measured by HF radar) distribution map. Units are centimeters per second, and degrees, respectively. The ocean current speed is 46.5 cm/s and the corresponding current direction is 177.2° at buoy #LKWF1.

Table 2. Winds retrieved from fully polarimetric SAR images and NDBC buoy #LKWF1, ocean surface currents measured by HF radar and retrieved ocean currents. Parameters of four kinds of data are simultaneous and collocated. Data are received on 19 January 2013.

	Sar Image	Buoy Data	Hf Radar	Retrieval Currents
Time	02:12	02:12	04:00	03:50
Site	26.602° N 80.145° W	26.613° N 80.034° W	26.587° N 80.098° W	26.613° N 80.034° W
Wind/current speed	Wind speed 10.52 m/s	Wind speed 8.9 m/s	Current speed 0.465 m/s	Current speed 0.380 m/s
Wind/current direction	Wind direction 41°	Wind direction 57°	Current direction 177.2°	Current direction 171°

4. Discussion

To make a better verification of the retrieval methodology for sea currents, 52 fully polarized SAR images are reselected for retrieval of the wind fields using the C-2PO model. Thereafter, the corresponding wind vector is determined from the buoy measurements and the data of the DWF fields are calculated. The retrieved east–west and the north–south sea components of the current speeds are compared to the current velocity measured by the HF radar data, and the current field vectors are constructed, as shown in Figure 9. The root-mean-square error of the sea current velocity calculated by the empirical formula given in Equations (7) and (8) is 12.42 cm/s and the error in the current direction is 6.32°. It is important to mention that the satellite retrieved ocean surface currents are only the wind-driven component of currents, and do not include the bulk currents, or wave induced currents such as Langmuir circulation and Stoke drift. In addition, wind driven currents require about one inertial period to come into balance with the winds; therefore these comparisons using instantaneous observations from satellite and buoys have additional variability (errors) because they are not always in equilibrium. For the 168 SAR images selected in this paper, the sea surface wind speeds are about 8–12 m/s, with the higher velocities, greater than 15 m/s, removed. This is because the effect of the ocean surface currents on wind fields retrieved from SAR images is more observable under moderate or low wind conditions. However, the C-2PO wind retrieval model is more applicable for moderate-to-high wind speeds, rather than low winds. In this paper, the retrieval methodology for sea surface currents is proposed for SAR images, also using wind vector data from buoy measurements and ocean surface currents measured by HF radar. It is notable that the retrieval methodology is an empirical formula given in Equations (7) and (8). Since the magnitude of the ocean surface current is relatively small, a small error in calculation can generate a large difference in the final result. Therefore, its applicability and accuracy need to be further improved. In future studies, a highly accurate relation between the DWF and the ocean surface currents shall be based on more accurate experimental field data observations, on a more accurate retrieval model for marine winds, as well as on the dynamical modelling of the interactions between the currents and the winds.

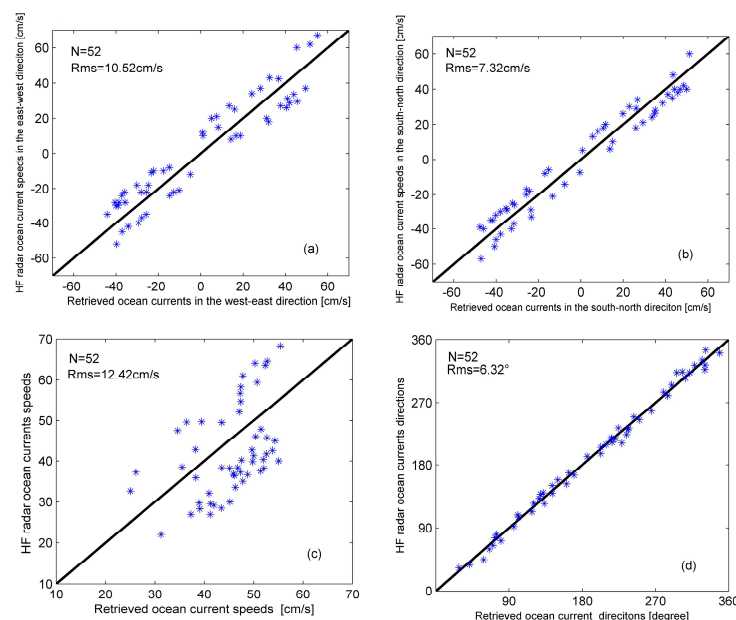


Figure 9. (a) Retrieved ocean surface current speeds in the east–west direction from empirical formulae given in Equations (7) and (8) versus HF radar measurements; (b) Retrieved sea current speeds of south–north direction from empirical formulae in Equations (7) and (8) versus HF radar measurements; (c) Synthetic current speeds in the east–west and south–north direction versus HF radar measurements; (d) Synthetic current directions versus HF radar measurements.

5. Conclusions

In this paper, we first use 168 full polarimetric SAR images from RADARSAT-2, apply the C-2PO wind retrieval model and CMOD5.N GMF as well as wind direction ambiguity removal methods to retrieve the ocean surface wind vectors. Applying the corresponding ocean currents from HF radar measurements and vector winds from buoy observations, we use vector analysis to explore the effect of ocean currents on the retrieval of wind fields from SAR images. The results suggest that when current speeds and directions are taken into consideration, the accuracy of wind speeds retrieved from SAR images is improved by about 0.3 m/s and wind directions are improved by about 3°. Thus, we present empirical Equations (7) and (8) to estimate the ocean surface current speed from data collected by SAR fully polarimetric images, wind vectors measured by buoys, and currents measured by the HF radar system. Experimental results show that the retrieval formula using the DWF data method provide results in a good agreement with the ones given by the HF radar observed data. Furthermore, the main conclusion of this work is that the empirical formulae in Equations (7) and (8) can be considered a reliable tool for estimates of ocean surface currents under moderate and low wind speed conditions (5–15 m/s) as provided by corresponding SAR images.

Acknowledgments: This work was supported by the National Natural Science Foundation of China (41776181), the National Key Research and Development Program of China (2016YFC1401007), the Global Change Research Program of China (Grant No. 2015CB953901), the Canadian Program on Energy Research and Development, the Canadian Space Agency's DUAP program, and the USA Office of Naval Research, Code 322, "Arctic and Global Prediction", directed by Drs. Martin Jeffries and Scott Harper. (Grant number and Principal Investigator: Perrie, N00014-15-1-2611).

Author Contributions: Tao Xie conceived and designed the experiments. He Fang and Li Zhao performed the experiments. Jingsong Yang and Yijun He supervised the work. He Fang, Tao Xie, and William Perrie wrote the paper.

Conflicts of Interest: The authors declare no conflict of interest.

References

1. Klemas, V. Remote Sensing of Coastal and Ocean Currents: An Overview. *J. Coast. Res.* **2012**, *28*, 576–586. [[CrossRef](#)]
2. Zuckerman, S.; Anderson, S.P.; Stuart, G.; Cooper, C. Real-time Ocean Surface current measurements in the Gulf of Mexico. *IEEE Oceans* **2015**, 1–6. [[CrossRef](#)]
3. Paduan, J.D.; Washburn, L. High-Frequency Radar Observations of Ocean Surface Currents. *Annu. Rev. Mar. Sci.* **2013**, *5*, 115–136. [[CrossRef](#)] [[PubMed](#)]
4. Romeiser, R.; Breit, H.; Eineder, M.; Runge, H.; Flament, P. Current measurements by sar along-track interferometry from a space shuttle. *IEEE Trans. Geosci. Remote Sens.* **2005**, *10*, 2315–2324. [[CrossRef](#)]
5. Hansen, M.W.; Collard, F.; Dagestad, K.-F.; Johannessen, J.; Fabry, P.; Chapron, B. Retrieval of Sea Surface Range Velocities from Envisat ASAR Doppler Centroid Measurements. *IEEE Geosci. Remote Sens.* **2011**, *49*, 3582–3592. [[CrossRef](#)]
6. Toporkov, J.V.; Hwang, P.A.; Sletten, M.A.; Farquharson, G.; Perkovic, D.; Frasier, S.J. Surface Velocity Profiles in a Vessel's Turbulent Wake Observed by a Dual-Beam Along-Track Interferometric SAR. *IEEE Geosci. Remote Sens. Lett.* **2011**, *8*, 602–606. [[CrossRef](#)]
7. Qazi, W.A.; Emery, W.J.; Fox-Kemper, B. Computing Ocean Surface Currents over the Coastal California Current System Using 30-Min-Lag Sequential SAR Images. *IEEE Geosci. Remote Sens.* **2014**, *52*, 7559–7580. [[CrossRef](#)]
8. Perrie, W.; He, Y.; Li, H.; Fang, H.; Zhao, S.; Yu, W. Ocean surface wave measurements from fully polarimetric SAR imagery. *Sci. China Earth Sci.* **2015**, *10*, 1849–1861.
9. Perrie, W.; Xie, T. Gulf Stream thermal fronts detected by synthetic aperture radar. In Proceedings of the IEEE International Geoscience & Remote Sensing Symposium, Honolulu, HI, USA, 25–30 July 2010.
10. Kuang, H.; Perrie, W.; Xie, T. Retrievals of sea surface temperature fronts from SAR imagery. *J. Geophys. Res. Lett.* **2012**, *10*, 1–7. [[CrossRef](#)]

11. Kelly, K.A.; Dickinson, S.; McPhaden, M.J.; Johnson, G.C. Ocean currents evident in satellite wind data. *J. Geophys. Res. Lett.* **2001**, *28*, 2469–2472. [[CrossRef](#)]
12. Zhang, F.W.; Drennan, W.M.; Haus, B.K. On wind-wave-current interactions during the Shoaling Waves Experiment. *J. Geophys. Res. Oceans* **2009**, *14*, 287–295. [[CrossRef](#)]
13. Small, R.J.; Richards, K.J.; Xie, S.P. Damping of Tropical Instability Waves caused by the action of surface currents on stress. *J. Geophys. Res.* **2009**, *114*, 553–556. [[CrossRef](#)]
14. O'Neill, L.W.; Chelton, D.B.; Esbensen, S.K. High-Resolution Satellite Measurements of the Atmospheric Boundary Layer Response to SST Variations along the Agulhas Return Current. *J. Clim.* **2005**, *14*, 2706–2723. [[CrossRef](#)]
15. Xie, T.; Zhao, D.; Perrie, W.; Fang, H. Electromagnetic backscattering from one-dimensional drifting fractal sea surface I: Wave-current coupled model. *Chin. Phys. B* **2016**, *4*, 79–102. [[CrossRef](#)]
16. Xie, T.; Perrie, W.; Zhao, D.; Fang, H. Electromagnetic backscattering from one-dimensional drifting fractal sea surface II: Electromagnetic backscattering model. *Chin. Phys. B* **2016**, *6*, 64–101. [[CrossRef](#)]
17. MacDonald, Dettwiler and Associates (MDA). *Radarsat-2 Product Description*; MDA: Richmond, BC, Canada, 2015.
18. Kohut, J.T.; Glenn, S.M.; Chant, R.J. Seasonal current variability on the New Jersey inner Shelf. *J. Geophys. Res.* **2013**, *109*. [[CrossRef](#)]
19. Emery, B.M.; Washburn, L.; Harlan, J.A. Evaluating radial current measurements from CODAR High-frequency radars with moored current meters. *J. Atmos. Ocean. Technol.* **2004**, *21*, 1259–1271. [[CrossRef](#)]
20. Liu, Y.; Weisberg, R.H.; Merz, C.R. Assessment of CODAR and WERA HF radars in mapping currents on the West Florida Shelf. *J. Atmos. Ocean. Technol.* **2014**, *31*, 1363–1382. [[CrossRef](#)]
21. Shen, Z.; Wu, X.; Lin, H.; Chen, X.; Xu, X.; Li, L. Spatial Distribution Characteristics of Surface Tidal Currents in the Southwest of Taiwan Strait. *J. Ocean Univ. China* **2014**, *13*, 971–978. [[CrossRef](#)]
22. Harlan, J.; Terrill, E.; Hazard, L.; Otero, M.; Roarty, H. The Integrated Ocean Observing System HF radar network. In Proceedings of the IEEE Washington OCEANS'15 MTS, Washington, DC, USA, 19–22 October 2015.
23. Temll, E.; Otero, M.; Hazard, L.; Conlee, D.; Harlan, J.; Kohut, J.; Reuter, P.; Cook, T.; Harris, T. Lindquist. Data Management and Real-time Distribution in the HF-Radar National Network. In Proceedings of the IEEE Oceans, Boston, MA, USA, 18–21 September 2006.
24. Hwang, P.A.; Zhang, B.; Toporkov, J.V.; Perrie, W. Comparison of composite Bragg theory and quad-polarization radar backscatter from RADARSAT-2: With application radar backscatter from RADARSAT-2: With applications to wave breaking and high wind retrieval. *J. Geophys. Res.* **2010**, *C8*, 246–255.
25. Vachon, P.W.; Wolfe, J. C-Band Cross-Polarization Wind Speed Retrieval. *IEEE Geosci. Remote Sens. Lett.* **2011**, *3*, 456–459. [[CrossRef](#)]
26. Zhang, B.; Perrie, W. Cross-Polarized Synthetic Aperture Radar: A New Potential Measurement Technique for Hurricanes. *Bull. Am. Meteorol. Soc.* **2012**, *93*, 531–541. [[CrossRef](#)]
27. Hersbach, H. Comparison of C-band scatterometer CMOD5.N equivalent neutral winds with ECMWF. *J. Atmos. Ocean. Technol.* **2010**, *4*, 721–736. [[CrossRef](#)]
28. Yueh, S.H.; Kwok, R.; Nghiem, S.V. Polarimetric scattering and emission properties of targets with reflection symmetry. *J. Radio Sci.* **2016**, *29*, 1409–1420. [[CrossRef](#)]
29. Yueh, S.H. Modeling of Wind Direction Signals in Polarimetric Sea Surface Brightness Temperatures. *J. IEEE Geosci. Remote Sens.* **1995**, *35*, 1400–1418. [[CrossRef](#)]
30. Tsai, W.Y.; Nghiem, S.V.; Huddleston, J.N. Polarimetric scatterometry: A promising technique for improving ocean surface wind measurements from space. *J. IEEE Geosci. Remote Sens.* **2000**, *38*, 1903–1921. [[CrossRef](#)]
31. Zhang, B.; Perrie, W.; Vachon, P.W. Ocean Vector Winds Retrieval from C-Band Fully Polarimetric SAR Measurements. *IEEE Geosci. Remote Sens.* **2012**, *11*, 4252–4261. [[CrossRef](#)]

